Letter

Observation of the skyrmion side-face state in a chiral magnet

Xiaodong Xie,[1,*] Kejing Ran,[1,*] Yizhou Liu,[2] Raymond Fan,[3] Wancong Tan,[1] Haonan Jin,[1] Manuel Valvidares,[4] Nicolas Jaouen,[5] Haifeng Du,[6,†] Gerrit van der Laan,[3] Thorsten Hesjedal,[7] and Shilei Zhang[1,‡]

[1]*School of Physical Science and Technology, ShanghaiTech University, Shanghai 201210, China; and ShanghaiTech Laboratory for Topological Physics, ShanghaiTech University, Shanghai 200031, China*

[2]*RIKEN Center for Emergent Matter Science (CEMS), Wako, Saitama 351-0198, Japan*

[3]*Diamond Light Source, Harwell Science and Innovation Campus, Didcot OX11 0DE, United Kingdom*

[4]*ALBA Synchrotron Light Source, Barcelona, E-08290, Spain*

[5]*Synchrotron SOLEIL, Gif-sur-Yvette, France*

[6]*The Anhui Key Laboratory of Condensed Matter Physics at Extreme Conditions, High Magnetic Field Laboratory and University of Science and Technology of China, Chinese Academy of Science (CAS), Hefei, Anhui Province, China*

[7]*Clarendon Laboratory, Department of Physics, University of Oxford, Parks Road, Oxford OX1 3PU, United Kingdom*

(Received 15 May 2022; revised 28 November 2022; accepted 24 January 2023; published 7 February 2023)

We identify a three-dimensional skyrmion side-face state in chiral magnets that consists of a thin layer of modulated surface spirals and an array of phase-locked skyrmion screws. Such chiral spin structures lead to a characteristic X-shaped magnetic diffraction pattern in resonant elastic x-ray scattering, reminiscent of Photo 51 of the DNA double-helix diffraction. By measuring both thin plates and bulk Cu_2OSeO_3 crystals in the field-in-plane geometry, we unambiguously identify the modulated skyrmion strings by retrieving their chirality and helix angle. The breaking of the translational symmetry along the side faces suppresses the bulk-favored conical state, providing a stabilization mechanism for the skyrmion lattice phase that has been overlooked so far.

DOI: 10.1103/PhysRevB.107.L060405

Magnetic skyrmions are topologically ordered, swirling spin configurations, which extend into strings in three-dimensional (3D) space [1]. The study of skyrmion stabilization and evolution mechanisms has been a long-standing task [2–15], which is intimately related to singularity dynamics and topology-driven phase transitions [4,16–25]. Recently, it has been recognized that skyrmion order is able to energetically dominate over other competing phases by adjusting its 3D string configurations [9,10,17,19,22,26–39], providing a new perspective for studying their nucleation process.

Chiral magnets with broken inversion symmetry present a standard model system for investigating these issues [1,6]. For bulk samples, conical order appears as the ground state at elevated fields, whereby the skyrmion string lattice phase only exists in a narrow window of the temperature-field phase diagram [7,40]. In the field out-of-plane (FOP) geometry, the surprising experimental finding of a largely enhanced skyrmion stability region in surface-confined thin-plate chiral magnets [41,42] led to the concept of the *skyrmion surface state*.

For thin plates, the breaking of translational symmetry at the two surfaces becomes energetically dominant [43,44], providing an exotic stabilization mechanism for skyrmions [9]. The surface state is represented by a unique 3D skyrmion structure with modulated skyrmion helicity angle along the string, named the surface twist effect [9,10]. Later, this twisting effect was also confirmed in semi-infinite systems, i.e., at the surface of a bulk chiral magnet [29,30], suggesting that this is a universal skyrmion stabilization principle. Based on the idea of the surface twist originating from translational symmetry breaking [43–49], the existence of other boundary 3D states seems plausible.

The recent advances in 3D magnetic characterization techniques stimulated a broad study of skyrmions in a "hidden" geometry with field in-plane (FIP), i.e., in geometrically confined systems with the field applied perpendicular to the confinement direction [21,24,25,50–52]. Such a confinement can be experimentally realized either in thinned-down samples, i.e., in a double-confined geometry, or on a well-defined side face of a bulk chiral magnet, i.e., in a single-confined geometry. Indeed, for double-confined chiral magnets, the FIP skyrmion phase appears to be more stable than the FOP phase [24,52,53]. On the other hand, for semi-infinite systems, in-plane skyrmions can survive at the very top surface, leading to a largely broadened phase pocket [54]. These experimental observations strongly hint at the existence of an exotic *skyrmion side-face state* (SFS), which is not simply due to a boundary confinement effect, motivating our study presented in this Letter.

In chiral magnets, the magnetic exchange interaction with exchange stiffness A, the Dzyalozhinskii-Moriya interaction (DMI) with constant D, and the Zeeman term due to an external magnetic field $\mathbf{B}$ are competing interactions [6,40]. The energy density takes the form $w = A(\nabla \mathbf{m})^2 + D\mathbf{m} \cdot (\nabla \times \mathbf{m}) - M_S \mathbf{B} \cdot \mathbf{m}$, where $\mathbf{m}$ is the local magnetization unit

*These authors contributed equally to this work.
†duhf@hmfl.ac.cn
‡shilei.zhang@shanghaitech.edu.cn

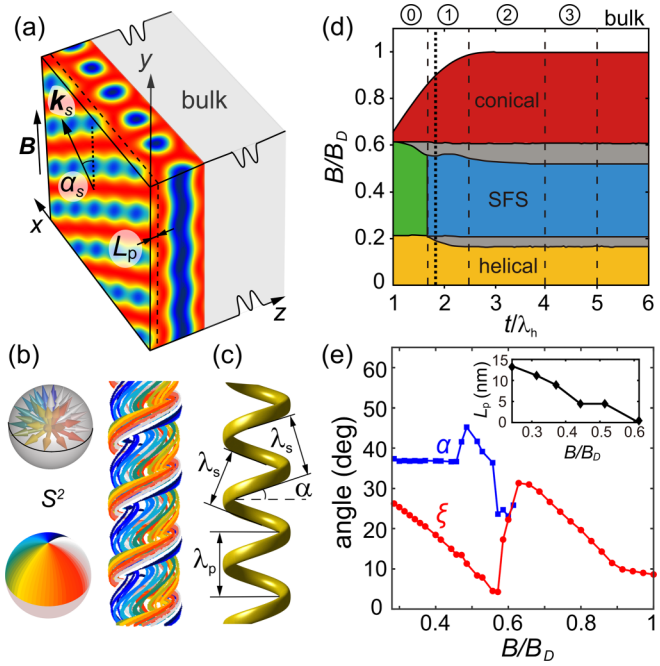

FIG. 1. (a) SFS at the side of a chiral bulk magnet. The color scale represents the m_y component of the magnetization. (b) Preimage representation of a skyrmion screw. (c) In the isosurface plot for $m_y = 0.9$, the definition of the screw parameters α (helix angle), λ_s (thread spacing), and λ_p (pitch) is given. (d) Thickness-field phase diagram for the side-face region, obtained from simulations. The green area only hosts the spiral side-face state, while the gray regions correspond to a mixed state of the two neighboring phases. For details, see Sec. S6 in Ref. [55]. The numbers on the top indicate the maximum number of skyrmion rows that can be supported. The dotted line at $t/\lambda_h = 1.83$ indicates the phase boundaries for a $t = 110$ nm system. (e) Plot of the helix angle α and the cone angle ξ as a function of field for a $t = 110$ nm system. The inset shows the field dependence of L_p.

vector, normalized by the saturation magnetization M_S. The ground state of the system with $B = 0$ is a helical state with incommensurate modulation periodicity $\lambda_h = 4\pi A/D$. Upon applying a magnetic field $< B_D$, where $B_D = D^2/2M_S A$, the magnetic propagation wave vector $\mathbf{k}_h$ becomes aligned along $\mathbf{B}$, and the modulation picks up a polarization component of $\cos\xi$, forming the conical state, where $0^\circ < \xi < 90^\circ$ is the cone angle. Consequently, another ingredient has to be introduced to stabilize the skyrmions over the conical phase.

Here, we introduce the terminating side face as a new ingredient for the stabilization of lateral skyrmions. First, we performed micromagnetic simulations to understand the structural features of the SFS by setting up a system with periodic boundary conditions in x and y, and open ones in z (see Sec. S1 in Ref. [55]). Figure 1(a) shows the magnetization distribution of the SFS for a moderate applied field and relatively large boundary layer thickness t. Upon closer inspection, we find that the SFS consists of two layers, i.e., a *spiral side-face modulation* state as the skin and a 3D *skyrmion screw* array that is attached to it (see details in Sec. S2 in Ref. [55]). The spiral side-face configuration shares similarities with the stacked spiral state [36,56] reported earlier for the FOP geometry. Here, along the y direction, the modulation can be regarded as a mixture of the 1D standard conical propagation and a cycloidal-type spiral. Such a magnetic wave undergoes a continuous phase shift along x, establishing a tilted wave vector $\mathbf{k}_s$ with an angle α_s. The spiral skin state has a penetration depth L_p beneath which the skyrmion screw array exists. This skyrmion screw array resembles the recently discussed metastable, non-axiosymmetric 3D skyrmion state with attractive interskyrmion potential [27,28,31,32]. This attractive potential may lead to their condensation into clusters or arrays [37,39,57].

Figure 1(b) shows the preimage bundles for a skyrmion screw. The preimage [58], i.e., the colored fibers that connect at infinity, correspond to distinct vectors on the S^2 order parameter space sphere, which are illustrated by the directional vectors (above) and the color-coded equatorial positions (below). Unlike standard skyrmion strings that have all preimage fibers aligned vertically, the skyrmion screw is formed by multiple helices with uniform chirality. In the simplified image of the screw in Fig. 1(c), the key parameters are illustrated. First, the pitch λ_p is identical for all other fibers. Its value is close to λ_h at lower fields. Second, the helix angle α is indicated, which is governed by λ_p [55]. Different fibers within the bundle have slightly different α values, and their average ranges from $\sim 20^\circ$–40°. Note that the cone angle ξ only affects the "flight width" of the screw, and not α itself [55]. To conclude, the key signatures of the SFS are a finite 3D skyrmion screw helix angle α with a fixed chirality, as well as their condensation into an ordered array.

The formation of the SFS can be described by the following mechanism (for details see Sec. S2 in Ref. [55]). First, the spiral side-face skin can be understood as the 3D extension of the surface twist, i.e., the fact that the abruptly truncated side face leads to the conical instability [43,44], which is reconciled by an additional helicoidal modulation. Such a modulation provides a suitable environment for skyrmion screws to evolve as a local energetic equilibrium state. Details of the properties of skyrmion screws are given in Sec. S3 in Ref. [55]. In other words, the spiral side-face state serves as a precursor for cutting the thread of the skyrmion screw. The formation of such non-axiosymmetric skyrmions suppresses the conical state near the side face [28]. Second, individual screws are tightly bound together, forming an array that is seamlessly attached to the spiral side-face skin. In this scenario, all the energetic disadvantages resulting from the void regions in the skyrmion screws are filled by either spiral side-face modulations or neighboring phase-locking screws [39]. Consequently, the screw helix angle is inherited from its precursor skin state ($\alpha = \alpha_s$), and the spacing of the screw's thread $\lambda_s = 2\pi/k_s$ [Fig. 1(c)].

Figure 1(d) shows the magnetic phase diagram as a function of normalized thickness t/λ_h and field B/B_D. Note that the magnetic phases identified here only exist in the side-face regions. It is thus clear that as long as the sample is thick enough ($t > 1.66\lambda_h$) the SFS is always present as a stable state at moderate fields. Moreover, there exist mixed states between the helical state and the SFS around 0.2 B/B_D, as well as the SFS and the conical state around 0.6 B/B_D, indicating a second-order-type phase transition. By increasing t,

the number of skyrmion rows increases in a nonlinear fashion, suggesting that L_p is thickness dependent.

The detailed field evolution of the cone angle ξ, the helix angle α, and L_p for a 110-nm-thick system is shown in Fig. 1(e), using the material parameters of Cu_2OSeO_3 ($\lambda_h =$ 60 nm). At lower fields, α remains almost constant, while the pitch λ_p takes the same value as the conical propagation periodicity λ_h [56,57]. Moreover, with increasing external field, ξ and L_p monotonically decrease. Closer to the transition region at around 0.5 B/B_D, α fluctuates due to the "melting" of the skyrmion screws with nonuniform pitch λ_p for individual screws [56,57]. Meanwhile, ξ continues to decrease, until a sudden enhancement occurs, indicating the breakdown of the SFS phase and the onset of purely conical modulations. Note that ξ does not reach zero even at $B = B_D$ due to the surface twist effect [44].

Despite this insight from simulations, the direct experimental observation of the SFS remains challenging. The recent developments in skyrmion imaging techniques give access to skyrmions in the FIP geometry [21,24,25,52]. However, due to the minute modulation amplitudes of the skyrmion screws, real-space imaging has not provided unambiguous experimental evidence of this phase, i.e., the presence of a finite α value, the chirality of the screw helix, and their assembly into an array. In contrast, reciprocal space mapping using diffraction is more sensitive to helixlike structures with minute, yet well-defined periodic variations.

The paramount example for the power of diffraction experiments is the determination of the double-helix structure of DNA performed in 1953 [59]. For the first experiment, we used a transmission setup as illustrated in Fig. 2(a), where the incident, circularly polarized x-rays scatter from the helix screw structure and are detected by a CCD camera. For a fixed goniometer angle, the x-rays probe the two sets of screw spacings, i.e., the two sets of oppositely inclined planes that appear when projecting the helix perpendicular to its axis [Fig. 1(b)], leading to the characteristic X-shaped diffraction pattern. Therefore, analyzing the X-shape directly reveals the key parameters of the skyrmion screw, namely, k_s and α, as illustrated in Fig. 2(a). Note that we are limited to first-order diffraction spots along the branches that make up the X-shape [the positions of the second-order spots are indicated in red in Fig. 2(a)].

Here, we use resonant elastic x-ray scattering (REXS) with photon energy near the Cu L_3 edge to study the magnetic phase in Cu_2OSeO_3 [60]. The magnetic field is applied along the y axis [Fig. 2(a)], and the sample can be rocked around the goniometer axis by ω. For the study of the SFS in the double-confined system, we use 110-nm-thick Cu_2OSeO_3 plates in the REXS transmission geometry, i.e., $\omega = 90°$ and $2\theta = 0°$. For the study of the SFS on the surface of a semi-infinite system, we use a Cu_2OSeO_3 bulk single crystal in the REXS reflection geometry, i.e., $\omega \approx 48°$ and $2\theta \approx 96°$, to reach a structural Bragg peak. In either case, a careful surface treatment is performed in order to optimize the crystalline quality of the surfaces (Sec. S4 in Ref. [55]), which is a key requirement for stabilizing the SFS. Circular dichroism is performed in the reflection geometry (CD-REXS), in order to retrieve the chiral information of the magnetic order [29]. The CD-REXS process is explained in detail in Sec. S5 of Ref. [55], along with a discussion of the expected contrast for all magnetic phases in the system.

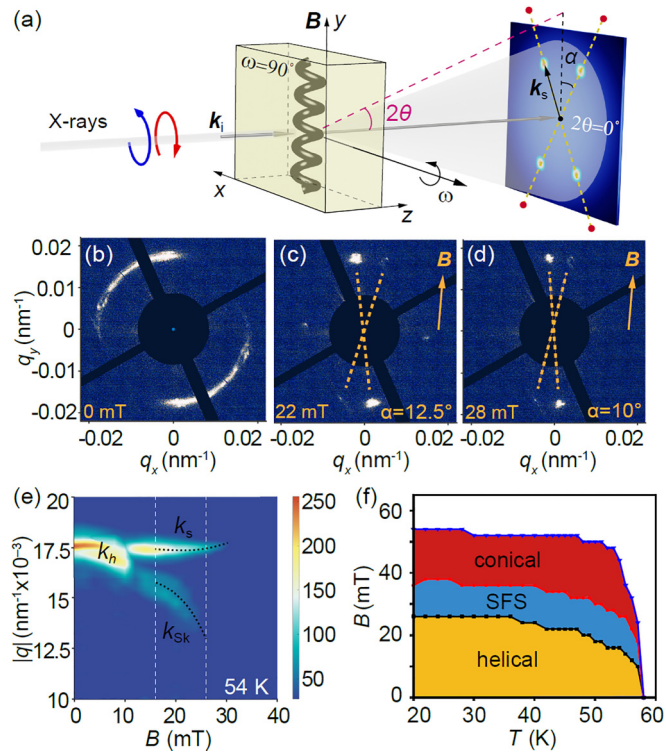

FIG. 2. (a) Schematics of the REXS setup. The coordinate system refers to the sample coordinates. (b)–(d) REXS patterns in transmission geometry of 110-nm-thick Cu_2OSeO_3 measured at 54 K for increasing applied field from 0 to 28 mT. (e) Magnetic scattering wave vector–magnetic field ($|q|$-B) REXS intensity map measured at 54 K. (f) Magnetic phase diagram derived from REXS data. The phase boundaries (at low temperature) can be compared with the simulated data ("bulk" region) shown in Fig. 1(d).

At higher angles with 2θ close to 90°, the intrinsic structural chirality leads to the opposite CD sign for the Friedel pair. In transmission geometry, on the other hand, the CD pattern smears out, preventing us from using CD-REXS to measure the chirality [55].

We first study the SFS in 110-nm-thick Cu_2OSeO_3 using the transmission setup, with the FIP applied along an arbitrary crystalline orientation. Figure 2(b) shows the REXS pattern for the helical state at 54 K [61]. At the same temperature, upon increasing the field to 22 mT, a diffraction pattern characteristic of the SFS emerges [Fig. 2(c)]. First, the two horizontal peaks are unique signatures of the formation of the skyrmion array [55]. The measured wave vector k_{Sk} corresponds to a periodic spacing of 66.7 nm. Strikingly, an X-shaped peak configuration appears, suggesting a screw-induced magnetic diffraction scenario, akin to the x rays probing a DNA-like double-helix. From its orientation, α and λ_s are obtained to be ~12.5° and ~58 nm, respectively. This leads to $\lambda_p = \lambda_s \cos\alpha = 56.6$ nm, which is equal to the intrinsic λ_h value measured for this material [54]. This result is consistent with our simulations, in which we find that $\lambda_p = \lambda_h$ at lower fields.

Note that one would expect equal intensity for the four X-peaks; however, we observe that one pair is stronger than the other. This is due to the additional signal of the spiral side-face modulation skin from one of the two confining surfaces. As the spiral side-face state shares the same $\mathbf{k}_s$ and α, its subsequent diffraction peaks overlap with those of the skyrmion screws. On the other hand, an increasing magnetic field drives the SFS into a transition region before entering the conical phase region, suggested by the disappearance of the horizontal peaks in Fig. 2(d) [55]. The pure X-peak pattern corresponds to the melting of the skyrmion screws, exhibiting a disordered skyrmion configuration, as well as a fluctuating λ_p. Consequently, a reduced α of 10° is observed.

As shown in Fig. 2(e), at 54 K, k_s is almost field independent, while k_{Sk} decreases with increasing field, meaning that the skyrmion lattice spacing gradually increases. The increased skyrmion-skyrmion distance reflects the fact that the interskyrmion potential tends to become repulsive [32], and thus the screw structure becomes energetically unfavored. Consequently, the screw's pitch increases [56,57], as if the coil was "softened," leading to a reduction in α. The experimental equilibrium phase diagram is summarized in Fig. 2(f), which is in agreement with our simulations shown in Figs. 1(d) and 1(e) (the phase boundaries for the $t = 110$ nm sample are indicated by a dashed line and the bulk limit is reached at $t/\lambda_{\mathrm{h}} \geqslant 6$). Note that the narrow SFS–conical transition region was also included in the conical phase. The phase diagram clearly shows that the SFS indeed gains stability as witnessed by its spreading into the conical phase region.

Next, we study the SFS at the surface of a bulk sample in the reflection geometry. The crystal was oriented with {001} along z, and field along y, which was chosen to be an orientation not coinciding with an in-plane {100} orientation [13]. In such a geometry, the probing depth is only a few tens of nanometers [30], which is ideally suited for the study of magnetic side-face structures. Figure 3(a) shows the CD-REXS pattern measured at 40 K and 18 mT, at which one would expect the conical phase in the bulk. Surprisingly, the diffraction pattern clearly marks the emergence of the SFS [labeled as phase (i)] at such a low temperature, indicating the robustness of the skyrmions on the side face. First, the horizontal peaks reveal the formation of the surface skyrmion lattice. Second, the X-shaped peaks can be identified with α measuring 31.5° and $\lambda_s = 58.6$ nm. Interestingly, a clear dichroic feature can be found as each pair has the opposite CD sign for $\pm q$. By performing the CD-REXS analysis, the chirality of the skyrmion screws can be determined to be left-handed [55]. The screw chirality is consistent with the handedness of the skyrmions from the same sample, confirming that the global chirality is inherited from the DMI.

Figure 3(b) shows the CD-REXS pattern at the same temperature in a field of 25 mT. Different from the behavior of the thin-plate sample, the SFS pattern suddenly changes to two orthogonal sets of peaks, accompanied by an abrupt change of α to zero [labeled as (ii)]. Indeed, by increasing the field, the SFS tends to enter the conical phase, featured by the two vertical peaks. Nevertheless, at $B < B_D$, axiosymmetric skyrmions can survive in a conical background with a modified modulation type [26] [inset to Fig. 3(b)]. Such a magnetic configuration was also obtained as a metastable state

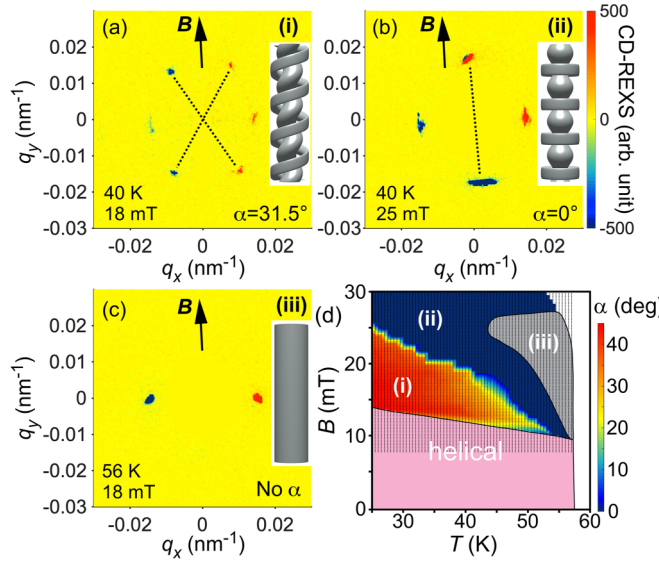

FIG. 3. (a)–(c) CD-REXS patterns of the magnetic phases characteristic for the side face of bulk Cu_2OSeO_3, i.e., (a) the SFS [labeled (i)], (b) the SFS with axiosymmetric skyrmion string modulations embedded in the conical phase [labeled (ii)], and (c) the in-plane skyrmion phase [labeled (iii)]. The insets to the panels illustrate the modulation mode of the magnetic states. (d) SFS phase diagram. The small black dots along lines of constant T represent the data points in the field-temperature space at which REXS measurements were carried out (between 8 and 30 mT and 25 and 58 K). Each point is colored depending on the measured α of the SFS [outside the SFS phase pocket, α is not defined and the point is left blank, see panel (c)]. A finite α (of up to ~40°) is found in the red region (i) of the phase diagram, corresponding to the SFS shown panel (a). In contrast, the blue region ($\alpha = 0°$) corresponds to the SFS phase (ii) with axiosymmetric skyrmion string modulations embedded in the conical phase [see panel (b)]. Below the SFS phase, the helical phase dominates. The pink area at high temperatures just below the transition temperature represents the bulk skyrmion lattice phase (iii) as obtained by superconducting quantum interference device (SQUID) measurements.

in our simulations [55]. Moreover, as shown in Fig. 3(c), at higher temperatures close to the bulk skyrmion lattice phase, α completely disappears, indicating the formation of the typical skyrmion lattice that consists of straight skyrmion strings [labeled (iii)].

Figure 3(d) shows the equilibrium phase diagram as mapped out by REXS. As a comparison, the bulk skyrmion lattice phase for the same crystal is marked by the gray pocket, measured by SQUID. It is thus clear that at the side face, the conically dominated area of the bulk state is replaced by the SFS, emphasizing its unique stability. The skyrmion-related phase pocket is composed of three regions, characterized by the three distinct diffraction patterns shown in Figs. 3(a)–3(c). For the SFS with finite α, the helix angle is almost field independent at lower field and undergoes a sudden change to zero when entering into the axiosymmetric, modulated skyrmion string lattice state. The field-dependent helix angle evolution is in good agreement with our theoretical expectations.

Nevertheless, in our simulation, the zero-α skyrmion string lattice is only metastable, while the conical order has the

lowest energy. Therefore, the existence of such a superposition phase indicates additional energy terms leading to its stabilization. While the extra terms for its equilibrium formation require further investigations, we postulate that magnetic anisotropies may be a necessary ingredient, as suggested by the temperature-dependent area of the phase diagram for the zero-α skyrmion state [blue area in Fig. 3(d)]. This is also consistent with the existence of the straight skyrmion string lattice phase that is observed as an extension of the bulk skyrmion lattice phase in the phase diagram. In fact, it was proposed that additional anisotropy effectively turns a straight skyrmion string lattice into a stable state [2,62].

In summary, by performing magnetic diffraction on the single- and double-confined chiral magnet Cu_2OSeO_3, we obtained the key experimental evidence of the existence of the SFS, i.e., the skyrmion screws' chirality, their helix angle α, as well as their condensation phase out of which the surface-attached array forms. The SFS is representative of an alternative skyrmion stabilization mechanism that is universal to all chiral magnets, also explaining the recent observed enhanced stability of in-plane skyrmions. Its existence further indicates that topological order may exist under more relaxed conditions on the side face compared to the bulk and can shed new light on the stabilization and morphology of skyrmions in other systems. The screwlike skyrmion structure in the FIP geometry may be utilized for advanced skyrmion-based devices due to their enhanced robustness and novel dynamics [27,54].

The REXS experiments were carried out in the RASOR endstation on beamline I10 at the Diamond Light Source (Proposals No. SI20437, No. MM26148, and No. MM22629). We acknowledge Synchrotron SOLEIL for providing the synchrotron radiation facilities (Proposal No. 20180618). Early experiments in support of these results were performed at the scattering endstation MARES of BOREAS beamline at theALBA Synchrotron (Proposal No. 2017092446). The Analytical Instrumentation Center SPST- AIC10112914 at ShanghaiTech University is acknowledged. This work was supported by the National Key R&D Program of China under Contract Nos. 2022YFA1403602 and 2020YFA0309400, the Science and Technology Commission of the Shanghai Municipality (Grant No. 21JC1405100), and the National Natural Science Foundation of China (Grants No. 12074257 and No. 12241406). K.J.R. acknowledges support from the National Natural Science Foundation of China (Grant No. 12004249) and the Shanghai Sailing Program (Grant No. 20YF1430600). Y.L. was supported by the RIKEN Special Postdoctoral Researcher Program (SPDR). T.H. acknowledges support from the Engineering and Physical Science Research Council (UK) under Grant No. EP/N032128/1.

[1] N. Nagaosa and Y. Tokura, Topological properties and dynamics of magnetic skyrmions, Nat. Nanotechnol. **8**, 899 (2013).
[2] A. N. Bogdanov and A. Hubert, Thermodynamically stable magnetic vortex states in magnetic crystals, J. Magn. Magn. Mater. **138**, 255 (1994).
[3] U. K. Rößler, A. N. Bogdanov, and C. Pfleiderer, Spontaneous skyrmion ground states in magnetic metals, Nature (London) **442**, 797 (2006).
[4] S. Mühlbauer, B. Binz, F. Jonietz, C. Pfleiderer, A. Rosch, A. Neubauer, R. Georgii, and P. Böni, Skyrmion lattice in a chiral magnet, Science **323**, 915 (2009).
[5] H. Wilhelm, M. Baenitz, M. Schmidt, U. K. Rößler, A. A. Leonov, and A. N. Bogdanov, Precursor Phenomena at the Magnetic Ordering of the Cubic Helimagnet FeGe, Phys. Rev. Lett. **107**, 127203 (2011).
[6] U. K. Rößler, A. A. Leonov, and A. N. Bogdanov, Chiral skyrmionic matter in non-centrosymmetric magnets, J. Phys.: Conf. Ser. **303**, 012105 (2011).
[7] S. Buhrandt and L. Fritz, Skyrmion lattice phase in three-dimensional chiral magnets from Monte Carlo simulations, Phys. Rev. B **88**, 195137 (2013).
[8] J. Sampaio, V. Cros, S. Rohart, A. Thiaville, and A. Fert, Nucleation, stability and current-induced motion of isolated magnetic skyrmions in nanostructures, Nat. Nanotechnol. **8**, 839 (2013).
[9] F. N. Rybakov, A. B. Borisov, and A. N. Bogdanov, Three-dimensional skyrmion states in thin films of cubic helimagnets, Phys. Rev. B **87**, 094424 (2013).
[10] A. O. Leonov, Y. Togawa, T. L. Monchesky, A. N. Bogdanov, J. Kishine, Y. Kousaka, M. Miyagawa, T. Koyama, J. Akimitsu, T. Koyama, K. Harada, S. Mori, D. McGrouther, R. Lamb, M. Krajnak, S. McVitie, R. L. Stamps, and K. Inoue, Chiral Surface Twists and Skyrmion Stability in Nanolayers of Cubic Helimagnets, Phys. Rev. Lett. **117**, 087202 (2016).
[11] C. Moreau-Luchaire, C. Moutafis, N. Reyren, J. Sampaio, C. A. F. Vaz, N. V. Horne, K. Bouzehouane, K. Garcia, C. Deranlot, P. Warnicke, P. Wohlhüter, J. M. George, M. Weigand, J. Raabe, V. Cros, and A. Fert, Additive interfacial chiral interaction in multilayers for stabilization of small individual skyrmions at room temperature, Nat. Nanotechnol. **11**, 444 (2016).
[12] A. K. Nayak, V. Kumar, Tianping Ma, P. Werner, E. Pippel, R. Sahoo, F. Damay, U. K. Rößler, C. Felser, and S. S. P. Parkin, Magnetic antiskyrmions above room temperature in tetragonal Heusler materials, Nature (London) **548**, 561 (2017).
[13] A. Chacon, L. Heinen, M. Halder, A. Bauer, W. Simeth, S. Mühlbauer, H. Berger, M. Garst, A. Rosch, and C. Pfleiderer, Observation of two independent skyrmion phases in a chiral magnetic material, Nat. Phys. **14**, 936 (2018).
[14] T. Kurumaji, T. Nakajima, M. Hirschberger, A. Kikkawa, Y. Yamasaki, H. Sagayama, H. Nakao, Y. Taguchi, T. Arima, and Y. Tokura, Skyrmion lattice with a giant topological Hall effect in a frustrated triangular-lattice magnet, Science **365**, 914 (2019).
[15] K. Karube, L. Peng, J. Masell, X. Yu, F. Kagawa, Y. Tokura, and Y. Taguchi, Room-temperature antiskyrmions and sawtooth surface textures in a non-centrosymmetric magnet with S4 symmetry, Nat. Mater. **20**, 335 (2021).
[16] P. Milde, D. Köhler, J. Seidel, L. M. Eng, A. Bauer, A. Chacon, J. Kindervater, S. Mühlbauer, C. Pfleiderer, S. Buhrandt,

C. Schütte, and A. Rosch, Unwinding of a skyrmion lattice by magnetic monopoles, Science **340**, 1076 (2013).

[17] F. N. Rybakov, A. B. Borisov, S. Blügel, and N. S. Kiselev, New Type of Stable Particlelike States in Chiral Magnets, Phys. Rev. Lett. **115**, 117201 (2015).

[18] J. Wild, T. N. G. Meier, S. Pöllath, M. Kronseder, A. Bauer, A. Chacon, M. Halder, M. Schowalter, A. Rosenauer, J. Zweck, J. Müller, A. Rosch, C. Pfleiderer, and C. H. Back, Entropy-limited topological protection of skyrmions, Sci. Adv. **3**, e1701704 (2017).

[19] F. Zheng, F. N. Rybakov, A. B. Borisov, D. Song, S. Wang, Z.-A. Li, H. Du, N. S. Kiselev, J. Caron, A. Kovács, M. Tian, Y. Zhang, S. Blügel, and R. E. Dunin-Borkowski, Experimental observation of chiral magnetic bobbers in B20-type FeGe, Nat. Nanotechnol. **13**, 451 (2018).

[20] Y. Liu, R. K. Lake, and J. Zang, Binding a hopfion in a chiral magnet nanodisk, Phys. Rev. B **98**, 174437 (2018).

[21] M. T. Birch, D. Cortés-Ortuno, L. A. Turnbull, M. N. Wilson, F. Grob, N. Träger, A. Laurenson, N. Bukin, S. H. Moody, M. Weigand, G. Schütz, H. Popescu, R. Fan, P. Steadman, J. A. T. Verezhak, G. Balakrishnan, J. C. Loudon, A. C. Twitchett-Harrison, O. Hovorka, H. Fangohr *et al.*, Real-space imaging of confined magnetic skyrmion tubes, Nat. Commun. **11**, 1726 (2020).

[22] K. Ran, Y. Liu, Y. Guang, D. M. Burn, G. van der Laan, T. Hesjedal, H. Du, G. Yu, and S. Zhang, Creation of a Chiral Bobber Lattice in Helimagnet-Multilayer Heterostructures, Phys. Rev. Lett. **126**, 017204 (2021).

[23] Y. Guang, K. Ran, J. Zhang, Y. Liu, S. Zhang, X. Qiu, Y. Peng, X. Zhang, M. Weigand, J. Gräfe, G. Schütz, G. van der Laan, T. Hesjedal, S. Zhang, G. Yu, and X. Han, Superposition of Emergent Monopole and Antimonopole in CoTb Thin Films, Phys. Rev. Lett. **127**, 217201 (2021).

[24] X. Yu, J. Masell, F. S. Yasin, K. Karube, N. Kanazawa, K. Nakajima, T. Nagai, K. Kimoto, W. Koshibae, Y. Taguchi, N. Nagaosa, and Y. Tokura, Real-space observation of topological defects in extended skyrmion-strings, Nano Lett. **20**, 7313 (2020).

[25] S. Seki, M. Suzuki, M. Ishibashi, R. Takagi, N. D. Khanh, Y. Shiota, K. Shibata, W. Koshibae, Y. Tokura, and T. Ono, Direct visualization of the three-dimensional shape of skyrmion strings in a noncentrosymmetric magnet, Nat. Mater. **21**, 181 (2022).

[26] A. N. Bogdanov and U. K. Rößler, Chiral Symmetry Breaking in Magnetic Thin Films and Multilayers, Phys. Rev. Lett. **87**, 037203 (2001).

[27] A. O. Leonov, J. C. Loudon, and A. N. Bogdanov, Spintronics via non-axisymmetric chiral skyrmions, Appl. Phys. Lett. **109**, 172404 (2016).

[28] A. O. Leonov, T. L. Monchesky, J. C. Loudon, and A. N. Bogdanov, Three-dimensional chiral skyrmions with attractive interparticle interactions, J. Phys.: Condens. Matter **28**, 35LT01 (2016).

[29] S. L. Zhang, G. van der Laan, W. W. Wang, A. A. Haghighirad, and T. Hesjedal, Direct Observation of Twisted Surface skyrmions in Bulk Crystals, Phys. Rev. Lett. **120**, 227202 (2018).

[30] S. Zhang, G. van der Laan, J. Müller, L. Heinen, M. Garst, A. Bauer, H. Berger, C. Pfleiderer, and T. Hesjedal, Reciprocal space tomography of 3D skyrmion lattice order in a chiral magnet, Proc. Natl. Acad. Sci. USA **115**, 6386 (2018).

[31] J. C. Loudon, A. O. Leonov, A. N. Bogdanov, M. C. Hatnean, and G. Balakrishnan, Direct observation of attractive skyrmions and skyrmion clusters in the cubic helimagnet Cu_2OSeO_3, Phys. Rev. B **97**, 134403 (2018).

[32] H. Du, X. Zhao, F. N. Rybakov, A. B. Borisov, S. Wang, J. Tang, C. Jin, C. Wang, W. Wei, N. S. Kiselev, Y. Zhang, R. Che, S. Blügel, and M. Tian, Interaction of Individual Skyrmions in a Nanostructured Cubic Chiral Magnet, Phys. Rev. Lett. **120**, 197203 (2018).

[33] A. O. Leonov and K. Inoue, Homogeneous and heterogeneous nucleation of skyrmions in thin layers of cubic helimagnets, Phys. Rev. B **98**, 054404 (2018).

[34] A. O. Leonov, A. N. Bogdanov, and K. Inoue, Toggle-switch-like crossover between two types of isolated skyrmions within the conical phase of cubic helimagnets, Phys. Rev. B **98**, 060411(R) (2018).

[35] H. R. O. Sohn, S. M. Vlasov, V. M. Uzdin, A. O. Leonov, and I. I. Smalyukh, Real-space observation of skyrmion clusters with mutually orthogonal skyrmion tubes, Phys. Rev. B **100**, 104401 (2019).

[36] G. P. Müller, F. N. Rybakov, H. Jónsson, S. Blügel, and N. S. Kiselev, Coupled quasimonopoles in chiral magnets, Phys. Rev. B **101**, 184405 (2020).

[37] S. M. Vlasov, V. M. Uzdin, and A. O. Leonov, Skyrmion flop transition and congregation of mutually orthogonal skyrmions in cubic helimagnets, J. Phys.: Condens. Matter **32**, 185801 (2020).

[38] F. Zheng, F. N. Rybakov, N. S. Kiselev, D. Song, A. Kovács, H. Du, S. Blügel, and R. E. Dunin-Borkowski, Magnetic skyrmion braids, Nat. Commun. **12**, 5316 (2021).

[39] A. O. Leonov, Skyrmion clusters and chains in bulk and thin-layered cubic helimagnets, Phys. Rev. B **105**, 094404 (2022).

[40] A. Bauer and C. Pfleiderer, Generic aspects of skyrmion lattices in chiral magnets, in *Topological Structures in Ferroic Materials: Domain Walls, Vortices and Skyrmions* (Springer International, Cham, 2016), pp. 1–28.

[41] X. Z. Yu, Y. Onose, N. Kanazawa, J. H. Park, J. H. Han, Y. Matsui, N. Nagaosa, and Y. Tokura, Real-space observation of a two-dimensional skyrmion crystal, Nature (London) **465**, 901 (2010).

[42] X. Z. Yu, N. Kanazawa, Y. Onose, K. Kimoto, W. Z. Zhang, S. Ishiwata, Y. Matsui, and Y. Tokura, Near room-temperature formation of a skyrmion crystal in thin-films of the helimagnet FeGe, Nat. Mater. **10**, 106 (2011).

[43] M. N. Wilson, E. A. Karhu, D. P. Lake, A. S. Quigley, S. Meynell, A. N. Bogdanov, H. Fritzsche, U. K. Rossler, and T. L. Monchesky, Discrete helicoidal states in chiral magnetic thin films, Phys. Rev. B **88**, 214420 (2013).

[44] S. A. Meynell, M. N. Wilson, H. Fritzsche, A. N. Bogdanov, and T. L. Monchesky, Surface twist instabilities and Skyrmion states in chiral ferromagnets, Phys. Rev. B **90**, 014406 (2014).

[45] H. Du, R. Che, L. Kong, X. Zhao, C. Jin, C. Wang, J. Yang, W. Ning, R. Li, C. Jin *et al.*, Edge-mediated skyrmion chain and its collective dynamics in a confined geometry, Nat. Commun. **6**, 9504 (2015).

[46] A. O. Leonov and M. Mostovoy, Edge states and skyrmion dynamics in nanostripes of frustrated magnets, Nat. Commun. **8**, 14394 (2017).

[47] X. Zhao, C. Jin, C. Wang, H. Du, J. Zang, M. Tian, R. Che, and Y. Zhang, Direct imaging of magnetic field-driven transitions

of skyrmion cluster states in FeGe nanodisks, Proc. Natl. Acad. Sci. U.S.A. **113**, 4918 (2016).

[48] J. Müller, Magnetic skyrmions on a two-lane racetrack, New J. Phys. **19**, 025002 (2017).

[49] C. Jin, Z.-A. Li, A. Kovács, J. Caron, F. Zheng, F. N. Rybakov, N. S. Kiselev, H. Du, S. Blügel, M. Tian, Y. Zhang, M. Farle, and R. E. Dunin-Borkowski, Control of morphology and formation of highly geometrically confined magnetic skyrmions, Nat. Commun. **8**, 15569 (2017).

[50] D. Wolf, S. Schneider, U. K. Rößler, A. Kovács, M. Schmidt, R. E. Dunin-Borkowski, B. Büchner, B. Rellinghaus, and A. Lubk, Unveiling the three-dimensional magnetic texture of skyrmion tubes, Nat. Nanotechnol. **17**, 250 (2022).

[51] K. Niitsu, Y. Liu, A. C. Booth, X. Yu, N. Mathur, M. J. Stolt, D. Shindo, S. Jin, J. Zang, N. Nagaosa, and Y. Tokura, Geometrically stabilized skyrmionic vortex in FeGe tetrahedral nanoparticles, Nat. Mater. **21**, 305 (2022).

[52] N. Mathur, F. S. Yasin, M. J. Stolt, T. Nagai, K. Kimoto, H. Du, M. Tian, Y. Tokura, X. Yu, and S. Jin, In-plane magnetic field-driven creation and annihilation of magnetic skyrmion strings in nanostructures, Adv. Funct. Mater. **31**, 2008521 (2021).

[53] H. Du, J. P. DeGrave, F. Xue, D. Liang, W. Ning, J. Yang, M. Tian, Y. Zhang, and S. Jin, Highly stable skyrmion state in helimagnetic MnSi nanowires, Nano Lett. **14**, 2026 (2014).

[54] S. Zhang, D. M. Burn, N. Jaouen, J.-Y. Chauleau, A. A. Haghighirad, Y. Liu, W. Wang, G. van der Laan, and T. Hesjedal, Robust perpendicular skyrmions and their surface confinement, Nano Lett. **20**, 1428 (2020).

[55] See Supplemental Material at http://link.aps.org/supplemental/10.1103/PhysRevB.107.L060405 for details on the micromagnetic simulations, the spiral side face state, skyrmion screws, the surface preparation and its effect on the SFS state, the CD-REXS process and the expected magnetic contrast, the determination of the magnetic phase diagram, and axiosymmetric skyrmion modulations, which includes Refs. [63–66].

[56] F. N. Rybakov, A. B. Borisov, S. Blügel, and N. S. Kiselev, New spiral state and skyrmion lattice in 3D model of chiral magnets, New J. Phys. **18**, 045002 (2016).

[57] A. O. Leonov, C. Pappas, and I. I. Smalyukh, Field-driven metamorphoses of isolated skyrmions within the conical state of cubic helimagnets, Phys. Rev. B **104**, 064432 (2021).

[58] P. J. Ackerman and I. I. Smalyukh, Static three-dimensional topological solitons in fluid chiral ferromagnets and colloids, Nat. Mater. **16**, 426 (2017).

[59] R. Franklin and R. G. Gosling, Molecular configuration in sodium thymonucleate, Nature (London) **171**, 740 (1953).

[60] S. L. Zhang, A. Bauer, H. Berger, C. Pfleiderer, G. van der Laan, and T. Hesjedal, Resonant elastic x-ray scattering from the skyrmion lattice in Cu_2 $OSeO_3$, Phys. Rev. B **93**, 214420 (2016).

[61] D. M. Burn, S. Wang, W. Wang, G. van der Laan, S. Zhang, H. Du, and T. Hesjedal, Field and temperature dependence of the skyrmion lattice phase in chiral magnet membranes, Phys. Rev. B **101**, 014446 (2020).

[62] M. N. Wilson, A. B. Butenko, A. N. Bogdanov, and T. L. Monchesky, Chiral skyrmions in cubic helimagnet films: the role of uniaxial anisotropy, Phys. Rev. B **89**, 094411 (2014).

[63] R. F. L. Evans, W. J. Fan, P. Chureemart, T. A. Ostler, M. O. A. Ellis, and R. W. Chantrell, Atomistic spin model simulations of magnetic nanomaterials, J. Phys.: Condens. Matter **26**, 103202 (2014).

[64] A. O. Leonov, T. L. Monchesky, N. Romming, A. Kubetzka, A. N. Bogdanov, and R. Wiesendanger, The properties of isolated chiral skyrmions in thin magnetic films, New J. Phys. **18**, 065003 (2016).

[65] G. van der Laan, Soft x-ray resonant magnetic scattering of magnetic nanostructures, C. R. Phys. **9**, 570 (2008).

[66] S. L. Zhang, A. Bauer, D. M. Burn, P. Milde, E. Neuber, L. M. Eng, H. Berger, C. Pfleiderer, G. van der Laan, and T. Hesjedal, Multidomain skyrmion lattice state in Cu_2OSeO_3, Nano Lett. **16**, 3285 (2016).